

**RUSSIAN ACADEMY of SCIENCE
KELDYSH INSTITUTE of APPLIED MATHEMATICS**

T.G. Yelenina, G.V. Ustyugova

**Mathematical simulation of the magnetic field coronal loop
evolution**

Moscow 2005

T.G. Yelenina, G.V. Ustyugova

Mathematical simulation of the magnetic field coronal loop evolution

Abstract

We present the results of the mathematical simulation of the interaction between a magnetic star and an accretion disk under finite disk magnetic diffusivity (or electric conductivity). It was found that this process occurs with quasi-periodic reconnection of the magnetic field coronal loops and plasmoid ejections. In the case of the perfect disk conductivity the evolution of the coronal magnetic field is due to the periodic outflow of angular momentum from the disk. In the case of a finite disk conductivity the configuration of the magnetic field is formed such that the total flux of angular momentum from the disk to the corona is not far from zero.

Contents

1	Introduction	3
2	Statement of the problem	4
3	Numerical method	12
4	Results	13
5	Conclusions	20

1 Introduction

This paper is devoted to the investigation of the evolution of the magnetic field linked with a magnetic star and its accretion disk. It is suggested that the plasma differential rotation along magnetic field lines is the reason of a "star – corona – disk" system evolution. These lines are anchored the star surface and the disk. The coronal plasma is perfect conductive. Since magnetic field lines are frozen to this ideal plasma, the differential rotation leads to magnetic field toroidal component generation. Magnetic pressure increases in corona inner parts and plasma is pushed towards the outer parts all together with the magnetic field lines frozen to this plasma. As a result there is deformation or even opening of poloidal magnetic field lines adopting a new configuration. The type of this new configuration is determined by several factors. One of them is the finite electrical conductivity of the relatively cold disk plasma.

It should be noted that the electroconductivity of the cosmic plasma is very high. We assume in this model that the plasma finite conductivity is essential only in the disk. The disk is formed by relatively dense and cold matter. The finite conductivity is determined by velocity turbulent fluctuations. The value of the turbulent conductivity and the turbulent magnetic diffusivity η_t (being both related) we consider as a parameter of the problem. To obtain an acceptable range for this parameter, it is supposed that the coefficient of the turbulent magnetic diffusivity agrees in order of magnitude with the turbulent kinematic diffusivity accepted in the standard α – model of Shakura – Sunyaev accretion disk [1]. Thus it is considered $\eta_t = \alpha_t c_s h$, where c_s is the sound speed in the disk, h – disk half-thickness, α_t – dimensionless coefficient varying in this range $0.01 \div 0.6$ [2].

We consider that the disk is Keplerian and cold. Under hydrostatic equilibrium, the Keplerian disk half-thickness h can be found from the relation [3]: $(h/r)^2 + b(h/r) - (c_s/V_k)^2 = 0$, where $b \equiv r(B_r^2 + B_\varphi^2)/(4\pi\Sigma V_k^2)$, Σ – surface density, V_k – Keplerian velocity, B_r , B_φ – magnetic field components.

In any case, even without taking into account the magnetic compression, the disk half-thickness satisfies the inequality $h \lesssim c_s/\Omega_k$, where Ω_k – Keplerian angle velocity. Therefore, turbulent magnetic diffusivity comes to $\eta_t \lesssim \alpha_t c_s^2/\Omega_k$.

The disk is cold, implying that its sound speed is much less than the Keplerian one. It means that $h \lesssim c_s/\Omega_k \ll r$, i.e. disk is geometrically thin. In this model, the disk is considered as a infinitely thin, rigid, conductive plane. It should be mentioned that disk has a complicated structure and its interaction with the magnetic field does not reduce to magnetic compression and magnetic field lines slippage relatively to matter [4]. All processes that take place in the disk with the assistance of both the plasma and the magnetic field we integrate in one phenomenological coefficient: the turbulent magnetic diffusivity η_t .

Besides the dynamics of the magnetic field, it is worthy to know its configuration after magnetic field lines opening. This configuration defines the disk and the magnetic field evolution at large time scales. The main factor influencing this evolution is the rate of angular momentum transfer from the disk. The leading hand in this process is also the magnetic field.

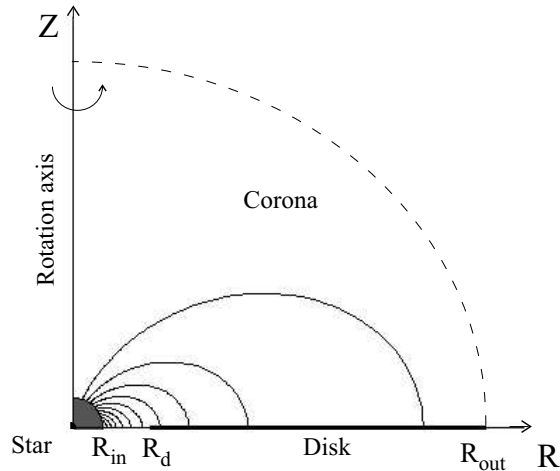


Figure 1: Sketch of the problem.

A sufficiently strong magnetic field can lead also to the formation of a matter outflow from the disk to the corona. In case of a thin Keplerian disk, a criterion for this outflow formation (in another words "wind") beginning has been given in [5]. To generate this outflow from a Keplerian disk, the magnetic field line should be inclined to the rotation axis with an angle of more than 30° , with that magnetic field line playing role of "rail" along which matter leaves the disk. Thus the final magnetic field configuration determines strongly both the rate of disk accretion, through the rate of angular momentum outflow, and the rate of matter outflow inclined to the rotation axis magnetic field lines.

In this paper, the evolution of the magnetic field configuration from an initial dipole-like topology into the final one is considered in the context of ideal MHD modeling. It is considered that the generated flow is axisymmetric and symmetric in relation with the equatorial plane. The dependence of the disk angular momentum outflow rate on the disk surface electrical conductivity is investigated.

We are deeply grateful to A.V. Koldoba and M.P. Galanin for very useful discussions.

This research received partial financial support from RFBR (grants 03—01—00461, 03—02—16548).

2 Statement of the problem

Let us consider a "star – corona – disk" system governed by the magnetic field (see figure 1). The star is a point source of gravity with mass M_* , magnetic moment μ_* and rotating with angular velocity Ω_* . It is assumed that the star rotation axis aligns with its magnetic axis z . Let us consider that the flow is axisymmetric. The disk rotating around the star is considered to be infinitely thin and located at $z = 0$. It is supposed that the disk is rotating following Keplerian

orbits around the star and the disk is finite conductive. The particle velocity in a Keplerian orbit with radius r is $V_k = \sqrt{GM_*/r}$, where $G = 0.667 \cdot 10^{-7} \text{cm}^3 \text{g}^{-1} \text{sec}^{-2}$ – gravitational constant. Thus, the disk is differential rotating.

The aim of this paper is to clear up the character of the magnetic field evolution and field topology depending on the disk magnetic diffusivity (or electric conductivity) at large time scales. Here λ is the surface electric conductivity and $\zeta = c^2/2\pi\lambda$ (c – speed of light) – surface magnetic diffusivity. As it will be shown below, it takes part into coupling conditions set on the equatorial plane $z = 0$.

It is known that coronal plasma electroconductivity is big enough to describe the flow by the system of the ideal MHD equations

$$\left\{ \begin{array}{l} \frac{\partial \rho}{\partial t} + \text{div } \rho \mathbf{u} = 0, \\ \frac{\partial \rho \mathbf{u}}{\partial t} + \text{div } \mathbf{T} = \rho \mathbf{g}, \\ \frac{\partial \mathbf{B}}{\partial t} - \text{rot } [\mathbf{u}, \mathbf{B}] = 0, \\ \frac{\partial \rho S}{\partial t} + \text{div } \rho S \mathbf{u} = 0, \\ \text{div } \mathbf{B} = 0. \end{array} \right. \quad (2.1)$$

Here $T_{ik} = \rho v_i v_k + p \delta_{ik} + \frac{1}{4\pi} \left(-B_i B_k + \frac{B^2}{2} \delta_{ik} \right)$ – the stress tensor; \mathbf{u} – the plasma velocity; \mathbf{B} – the magnetic field; ρ and p – the plasma density and pressure; $S = p/\rho^\gamma$ – the entropy function; γ – the adiabatic index; $\mathbf{g} = -\nabla \Phi_g$ – the gravitational acceleration; $\Phi_g = -GM_*/R$ – the star gravity potential; R – the distance from the gravitating center.

The system (2.1) is solved in spherical coordinates (R, φ, θ) , with θ being the polar angle with the symmetry axis. Velocity \mathbf{u} and magnetic field \mathbf{B} have all their components $\mathbf{u} = (u, v, w)$ and $\mathbf{B} = (B_R, B_\varphi, B_\theta)$ different from zero.

Dimensionless variables and typical quantities for

T Tauri stars

To make the dimensionless form of (2.1) is carried out in standard way. As distance scale, R_0 , we take one third of the distance from the star center to the inner edge of the disk. Thus, in dimensionless units the disk inner edge is $R_d = 3R_{in}$. The inner radius of the computation region in dimensionless units is $R_{in} = 1$. The time and the velocity scales are chosen such that in dimensionless units $GM_* = 1$. This requirement gives for the time scale $t_0 = \sqrt{R_0^3/GM_*}$ and for the velocity scale $v_0 = R_0/t_0$. As magnetic field scale, B_0 is taken and then density, pressure and magnetic moment scales are $\rho_0 = B_0^2/v_0^2$, $p_0 = B_0^2$, $\mu_{*0} = B_0 R_0^3$.

As typical quantities of T Tauri stars we adopt standard values like a star mass $M_* = 0.8M_\odot = 1.6 \cdot 10^{33}$ g, and a disk inner edge equal to $9M_\odot$, it is $5.4 \cdot 10^{11}$ cm. Therefore the

distance scale is $R_0 = R_d/3 = 1.8 \cdot 10^{11}$ cm, the time and velocity scales are $0.74 \cdot 10^4$ sec and $2.43 \cdot 10^7$ cm/sec respectively. The Keplerian rotation period at the disk inner edge is 8.3 days. The simulation region size is 0.0756 AU or $1.134 \cdot 10^{12}$ cm.

The star magnetic moment is taken such that the magnetic field on the star surface is 300 G, so $B_0 = 0.13$ G. Thus, on the disk inner part, the dipole magnetic field is 2.4 G, and the magnetic moment $-7.6 \cdot 10^{32} \text{G} \cdot \text{cm}^3$. The density scale is $2.88 \cdot 10^{-17} \text{g/cm}^3$, typical for the disks around T Tauri stars.

Selection of the electric conductivity

The value of the magnetic diffusivity is not known exactly. It could be suggested that turbulent diffusion of magnetic field is determined by the same processes that determine turbulent viscosity, which leads to angular momentum transport in the disk. Thus, it is assumed that turbulent magnetic viscosity η_t is in the order of kinematic turbulent viscosity like in the Shakura – Sunyaev model [1]: $\eta_t = \alpha_t c_s h$.

The turbulent electroconductivity $\sigma_t = \frac{c^2}{4\pi\eta_t} = \frac{c^2}{4\pi\alpha_t c_s h}$ is associated with the magnetic viscosity η_t .

The surface disk conductivity is $\lambda = \int \sigma_t dz \sim 2h\sigma_t = \frac{c^2}{2\pi\alpha_t c_s}$, and the surface magnetic viscosity is

$$\zeta = \frac{c^2}{2\pi\lambda} = \alpha_t c_s = \alpha_t \left(\frac{c_s}{V_k} \right) V_k.$$

In thin accretion disks $c_s/V_k = h/r \ll 1$. It is assumed related to the nondimensional coefficient α_t that it is about $0.01 \div 0.6$, like in Shakura – Sunyaev theory. Thus, an acceptable coefficient of the magnetic surface viscosity is $\zeta = (0.01 \div 0.6)(c_s/V_k)V_k$.

Initial conditions

Let us suggest that, at the initial time, the stellar magnetic field with dipole-like topology and magnetic moment μ_* penetrates the corona and the disk. In this case the components of the magnetic field \mathbf{B} are

$$B_R = \frac{2\mu_* \cos \theta}{R^3}, \quad B_\theta = \frac{\mu_* \sin \theta}{R^3}, \quad B_\varphi = 0.$$

At initial time $t = 0$, the matter of the corona and the disk is in mechanical equilibrium with the force-free dipole magnetic field, i.e. gravitational force is balanced with "centrifugal" force (liquid particle acceleration) and pressure gradient.

The momentum equation for the system (2.1) taking into account that particles follow circular orbits is

$$-\omega^2 r \mathbf{e}_r + \frac{1}{\rho} \nabla p = -\nabla \Phi_g, \quad (2.2)$$

where \mathbf{e}_r – a unit vector with the direction of the cylindrical radius $r = R \sin \theta$, that on disk surface it is $\theta = \pi/2$ and $r = R$.

It is not useful for the paper goals the case of a barotropic density distribution when density and pressure are connected by some dependence $\rho = \rho(p)$ and angular velocity depends only on the cylindrical radius r . This is due to the magnetic pressure $\mathbf{B}^2/8\pi$ of the dipole-like field \mathbf{B} decreases like $1/R^6$. Also, the most of the simulation region is occupied by a relatively dense plasma, where gas pressure dominates. This dense plasma prevents magnetic field line opening.

Let us consider a more general case supposing that density ρ is function not only of pressure p but also of cylindrical radius r : $\rho = \rho(r, p)$. Let us mark $V(p, r) = 1/\rho$. The momentum equation along the z axis (the projection of equation (2.2) to the z axis) is

$$V(p, r) \frac{\partial p}{\partial z} + \frac{\partial \Phi_g}{\partial z} = 0.$$

Integrating it by z it is obtained

$$\int_{p_0}^p V(p', r) dp' + \Phi_g = E(r). \quad (2.3)$$

To find the function $E(r)$ let us suggest that $p \rightarrow 0$ under $z \rightarrow \infty$. Since under $z \rightarrow \infty$ gravitational potential $\Phi_g \rightarrow 0$, making $z \rightarrow \infty$ in equation (2.3) gives $\int_{p_0}^0 V(p', r) dp' + 0 = E(r)$. Substituting this function $E(r)$ into equation (2.3), we can represent it in the following form:

$$\int_0^p V(p', r) dp' + \Phi_g = 0. \quad (2.4)$$

Here is assumed that integral is convergence on its inferior limit.

Let us consider now the momentum equation (2.2) along the radial direction

$$-\omega^2 r + V(p, r) \frac{\partial p}{\partial r} + \frac{\partial \Phi_g}{\partial r} = 0, \quad (2.5)$$

After differentiating equation (2.4) by r it is obtained

$$V \frac{\partial p}{\partial r} + \int_0^p \frac{\partial V}{\partial r} dp' + \frac{\partial \Phi_g}{\partial r} = 0. \quad (2.6)$$

Subtracting (2.5) from (2.6) it is found

$$\omega^2 r + \int_0^p \frac{\partial V}{\partial r} dp' = 0. \quad (2.7)$$

Thus, giving the function $V(p, r)$, the relation (2.4) defines the function $p(r, z)$ and relation (2.7) – function $\omega(r, z)$.

If $V(p, r) = k(r)/p^\alpha$, $\alpha = \text{const} < 1$ (this condition is essential for the integral convergence under $p \rightarrow 0$ in left part of equation (2.4)), then equations (2.4), (2.7) are

$$\begin{cases} \frac{kp^{1-\alpha}}{1-\alpha} + \Phi_g = 0, \\ \frac{p^{1-\alpha}}{1-\alpha} k' + \omega^2 r = 0. \end{cases}$$

Assuming $z = 0$ and excluding the pressure p it is found that $\frac{dk}{k} = \Omega^2 r \frac{dr}{\Phi_g}$, where $\Omega(r) = \omega(r, 0)$ – angular velocity at equatorial plane ($z = 0$). Integrating it, the function $k(r)$ has been found

$$\ln k = -\frac{1}{GM_*} \int \Omega^2(r) r^2 dr. \quad (2.8)$$

The angular velocity at the equatorial plane $z = 0$ is chosen because it is assumed that at small distances from the star $r \leq r_1$, the matter rotates with the angular velocity of the star: $\Omega = \Omega_*$. Under $r > r_2 > r_1$ the matter rotates by Keplerian orbits, i.e. $\Omega = \sqrt{GM_*/r^3}$. For radii between r_1 and r_2 the angular velocity Ω changes linear from star angular velocity to disk inner part angular velocity at $r = r_2$. The values r_1, r_2 are the parameters of the problem and are chosen by the following way: $r_1 = 2R_{in}$, $r_2 = 3R_{in}$. So,

$$\Omega(r) = \begin{cases} \Omega_* = \sqrt{GM_*/r_1^3}, & 0 < r < r_1, \\ \Omega_* + \frac{\sqrt{GM_*/r_2^3} - \Omega_*}{r_2 - r_1} (r - r_1), & r_1 < r < r_2, \\ \sqrt{GM_*/r^3}, & r > r_2. \end{cases} \quad (2.9)$$

As a result, the distributions of the pressure $p(r, z)$, density $\rho(r, z)$ and angular velocity $\omega(r, z)$ are obtained

$$p(r, z) = \left(\frac{1-\alpha}{k(r)} \frac{GM_*}{\sqrt{r^2+z^2}} \right)^{1/(1-\alpha)}, \quad \rho(r, z) = \frac{p^\alpha(r, z)}{k(r)}, \quad \omega = \sqrt{\frac{p^{1-\alpha}}{\alpha-1} \frac{k'(r)}{r}}.$$

Boundary conditions

As mentioned above, in the framework of our model we suggest that the disk is an infinitely thin conducting plane, at $z = 0$ (in cylindrical coordinates) or at $\theta = \pi/2$ (in spherical coordinates). The disk particles move along circular orbits with angular velocities $\Omega(r)$. Besides that, it is suggested that for a surface current in the disk, the Ohm's law is fulfilled

$$\mathbf{i} = \lambda \mathbf{E}'_D. \quad (2.10)$$

Where \mathbf{i} – current surface density; \mathbf{E}'_D – tangential to the disk electromotive force in comoving frame; λ – disk conductivity.

Formula (2.10) follows from integration over z the components of the relation $\mathbf{j} = \sigma_t \mathbf{E}'$ (standard Ohm's law). Here \mathbf{j} is current density, σ_t – plasma conductivity. Assuming that the

angular velocity ω and r, φ – components of electric field \mathbf{E}' change neglectable in z –direction on scales of the order of the disk thickness $2h$, we assume for the disk surface electric conductivity $\lambda = \int \sigma_t dz \sim 2h\sigma_t$.

From the assumption that corona plasma is perfect conductor, it follows that the electric field in the laboratory frame of the bound disk – corona is defined by the expression

$$\mathbf{E} = -\frac{1}{c}[\mathbf{u}, \mathbf{B}]_{z=0}, \quad (2.11)$$

where \mathbf{u} – the plasma velocity, \mathbf{B} – the magnetic field at $z = 0$.

Since the tangential components of electric field are continuous when crossing the bound between two media, the formula (2.11) gives the value of the electric field in the disk in the laboratory frame. At the comoving frame it has been found that $\mathbf{E}'_D = -\frac{1}{c}[\mathbf{u} - \mathbf{V}, \mathbf{B}]$, where \mathbf{V} – disk element velocity.

Then Ohm's law (2.10) becomes

$$\mathbf{i} = -\frac{\lambda}{c}[\mathbf{u} - \mathbf{V}, \mathbf{B}]. \quad (2.12)$$

On the other hand, surface currents in the disk (at $z = 0$) lead to a discontinuity in the tangential to the disk components of the magnetic field. Mathematically it means that the following condition is fulfilled [6]

$$[\mathbf{n}, \mathbf{B}_1 - \mathbf{B}_0] = \frac{4\pi}{c}\mathbf{i}, \quad (2.13)$$

where $\mathbf{B}_1, \mathbf{B}_0$ – the magnetic field under and over the disk, $\mathbf{n} = (-1, 0, 0)$ – unitary vector normal to the disk and downward half-space directed (see figure 2) in cylindrical coordinates.

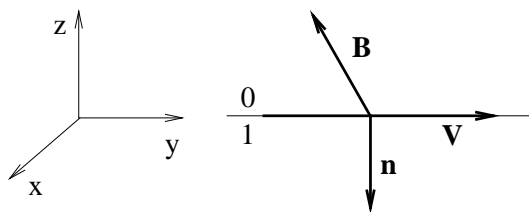


Figure 2: Directions of \mathbf{B} and \mathbf{n}

Since we suggest that MHD–flow is symmetric in relation to equatorial plane and consider the problem in the upper half-space, then $\mathbf{B}_0 = -\mathbf{B}_1 = \mathbf{B}|_{z=0}$ and (2.13) gives the following

$$[\mathbf{n}, \mathbf{B}] + \frac{2\pi}{c}\mathbf{i} = 0. \quad (2.14)$$

Substituting expression (2.12) into the equation (2.14) for current \mathbf{i} , finally it is found

$$[\mathbf{u} - \mathbf{V} - \zeta\mathbf{n}, \mathbf{B}] = 0, \quad (2.15)$$

where $\zeta = c^2/(2\pi\lambda)$ – the magnetic diffusivity.

In spherical coordinates the tangential components of (2.15) in the disk are

$$\begin{aligned} (v - V_k)B_\theta - (w - \zeta)B_\varphi &= 0, \\ uB_\theta - (w - \zeta)B_R &= 0. \end{aligned} \tag{2.16}$$

The relations (2.16), expressing Ohm's law for surface current in the disk, give two boundary conditions in the equatorial plane under $\theta = \pi/2$ ($z = 0$).

The real disk has some vertical (in z -direction) structure that is not considered here. It is essential that thermodynamic parameters of the disk plasma change in the vertical direction turning smoothly to the corona ones. So, the boundary conditions can be set arbitrarily, based on some physically reasonable assumptions.

We assume that matter flows from the disk to the corona at small velocity. Matter will flow from the Keplerian disk to the corona if the magnetic field line starting from the disk is inclined to the rotation axis by an angle larger than 30° with the poloidal plane. It could be expected that plasma leaves the disk with the velocity less than the slow magnetosonic one.

Let us accept that the z component of the velocity is a fraction α_c of the cusp one in this direction: $v_z = \alpha_c c_0$, $c_0^2 = \frac{c_s^2 a_z^2}{c_s^2 + a^2}$, where a_z – z -component Alfvén velocity, $\alpha_c(r) < 1$ – parameter of the problem.

The cusp velocity is not larger than slow magnetosonic one and with the same direction. Therefore, if taking into consideration that in the equatorial plane $w = -v_z$ and choosing $\alpha_c = \alpha_c(r) < 1$ then the condition (2.17) guarantees that the plasma outflow is not larger than the slow magnetosonic one, giving the third boundary condition for $\theta = \pi/2$:

$$w + \alpha_c(r) \frac{c_s |a_\theta|}{\sqrt{c_s^2 + a^2}} = 0. \tag{2.17}$$

The condition (2.17) guarantees also that from any point of the disk five characteristics come out: two entropic, slow, fast magnetosonic and Alfvén ones. So, one should set another two boundary conditions.

We assume that the specific entropy of the matter flowing out from the disk does not vary with time

$$S|_{\theta=\pi/2} = S_d(r).$$

This condition corresponds that matter outflow from the disk does not change its interior structure, i.e. the disk is enough large mass, energy and angular momentum tank.

To get the equation describing the evolution of the magnetic flux function on the disk (at $\theta = \pi/2$) let us use the induction equation

$$\frac{\partial B_\theta}{\partial t} + \frac{c}{R} \frac{\partial R E_\varphi}{\partial R} = 0. \tag{2.18}$$

Taking into account that on the disk $B_\theta|_{\theta=\pi/2} = \frac{1}{R} \frac{\partial \Psi}{\partial R}|_{\theta=\pi/2}$ and Ohm's law is fulfilled then the azimuth component of the surface current, $E_\varphi + \frac{c}{2\pi\sigma_t} B_R|_{\theta=\pi/2} = 0$. Integrating (2.18), we

found

$$\frac{\partial \Psi}{\partial t} + \zeta R B_R \Big|_{\theta=\pi/2} = 0.$$

Thus, two of boundary conditions are the Ohm's law for the surface currents

$$\begin{aligned} \phi_1 &= (v - V)B_\theta - (w - \zeta)B_\varphi = 0, \\ \phi_2 &= uB_\theta - (w - \zeta)B_r = 0. \end{aligned} \quad (2.19)$$

The third and fourth ones are

$$\phi_3 = w + \alpha_c c_0 = 0, \quad (2.20)$$

$$\phi_4 = S_d(r) = 0. \quad (2.21)$$

Differentiating (2.19) – (2.21) by t , four linear equations are obtained such that "vector" \mathcal{U}_t should satisfy them

$$\langle \Psi_k, \mathcal{U}_t \rangle = 0, \quad \Psi_k = \frac{\partial \phi_k}{\partial \mathcal{U}}, \quad k = 1, 2, 3, 4. \quad (2.22)$$

Hence, in the disk \mathcal{U}_t satisfies four equations (2.22) containing Ψ_k

$$\Psi_1 = \{\zeta B_\varphi - V B_\theta, 0, B_\theta, -B_\varphi, 0, \rho(\zeta - w), \rho(v - V), 0\},$$

$$\Psi_2 = \{\zeta B_R, B_\theta, 0, -B_R, \rho(\zeta - w), 0, \rho u, 0\},$$

$$\Psi_3 = \left\{ -\frac{\alpha_c}{2} c_0^2 (c_s^2 + \gamma a^2), 0, 0, c_0 (c_s^2 + a^2), \alpha_c c_0^2 \frac{B_R}{4\pi}, \alpha_c c_0^2 \frac{B_\varphi}{4\pi}, -\frac{\alpha_c c_0^2 (c_s^2 + a_\tau^2) B_\theta}{a_\theta^2} \frac{1}{4\pi}, -\frac{\alpha_c c_0^2}{2c_s^2} \gamma a^2 \rho^{\gamma-1} \right\},$$

$$\Psi_4 = \{-S, 0, 0, 0, 0, 0, 0, 1\},$$

where $a_\tau^2 = a_R^2 + a_\varphi^2$.

Additional equations are obtained from the system of equations written in quasi-linear form. Multiplying these equations by vectors \mathcal{L}_a corresponded to the characteristics coming to the disk there the additional equations are obtained for vector \mathcal{U}_t by definition

$$\langle \mathcal{L}_a, \mathcal{U}_t \rangle + \lambda_a \langle \mathcal{L}_a, \frac{1}{R} \frac{\partial \mathcal{U}}{\partial \theta} \rangle = \langle \mathcal{L}_a, Q \rangle, \quad \text{for } \lambda_a \geq 0, \quad (2.23)$$

where both right parts of the equations and items containing differentiation in radial direction

enter into Q . The items $\langle \mathcal{L}_a, \frac{1}{R} \frac{\partial \mathcal{U}}{\partial \theta} \rangle$ in the left side of (2.23) are approximated by directed differences against the flow. The solutions of equations (2.22), (2.23) may be found in the form of $\mathcal{U}_t = \sum_a \eta_a \mathcal{R}_a$, where $\eta_a = \langle \mathcal{L}_a, \mathcal{U}_t \rangle$. From (2.23), it is found that coefficients η_a , corresponding to $\lambda_a \geq 0$, are

$$\eta_a = -\lambda_a \langle \mathcal{L}_a, \frac{1}{R} \frac{\partial \mathcal{U}}{\partial \theta} \rangle + \langle \mathcal{L}_a, Q \rangle.$$

Substituting these η_a into (2.22), it is found the linear system for the rest η_a

$$\sum_{\lambda_a < 0} \langle \Psi_k, \mathcal{R}_a \rangle \eta_a = - \sum_{\lambda_a \geq 0} \langle \Psi_k, \mathcal{R}_a \rangle \eta_a, \quad k = 1, 2, 3, 4 \quad (2.24)$$

where at the left there is the sum by a such that $\lambda_a < 0$, at the right there is the sum by a where $\lambda_a \geq 0$. In the linear equation system (2.24), η_a is found by Gauss method.

Let us formulate the boundary conditions in the inner bound of the simulation region under $R = R_{in}$. As boundary conditions on equatorial plane, they are set for reasons of physical rationality. The main factor to take into account is on the one hand to choose arbitrary the place of the inner bound, i.e. the value of the inner radius of the simulation region R_{in} , and on the other hand quick like R^{-6} increasing magnetic pressure of stellar dipole-like field. R_{in} is chosen to be such that in some neighborhood of the inner bound, the star magnetic field has dominant influence on the plasma dynamics. In other words, in this region Alfvén velocity is much more than both the gas sound speed and the Keplerian one. On the other hand, the choice of a very small R_{in} is not reasonable from the computational point of view, since, into the simulation region, are the included parts of the magnetosphere where Alfvén velocity is too large, and it leads to an essential decreasing of time integration step. Since in the considered model it is assumed that magnetic field lines are frozen into the star surface rotating with angular velocity Ω_* , in the inner bound of the simulation region (and under it, right on the star surface) plasma moves along the rotating magnetic field lines. In the frame of the rotating star (on inner bound) plasma velocity vector is parallel to the magnetic field one. Since transforming to the rotating frame \mathbf{B} does not change, but \mathbf{u} transforms into $\mathbf{u} - V_* \mathbf{e}_\varphi$, where $V_* = \Omega_* R_{in} \sin \theta$, then this boundary condition can be written in the following way:

$$[\mathbf{u} - V_* \mathbf{e}_\varphi, \mathbf{B}]_{R=R_{in}} = 0. \quad (2.25)$$

Condition (2.25) implies also that in the rotating frame, the electric field in the inner bound is zero. The conditions (2.25) give two boundary conditions under $R = R_{in}$.

On the outer bound, at $R = R_{out}$, "free" boundary conditions are set. Such conditions should not influence on the solutions inside simulation region preventing poloidal magnetic field lines opening. As "free" conditions we take that wave strength coming into the region from the outer part become zero

$$\langle \mathcal{L}_a, \frac{\partial \mathcal{U}}{\partial R} \rangle \Big|_{R=R_{out}} = 0 \text{ for } \lambda_a \leq 0.$$

Here \mathcal{L}_a – left eigenvectors of characteristic matrix calculated in the radial direction.

On the rotation axis, although it is not a bound, symmetry of the flow conditions for this axis are set:

$$v = w = 0, B_\varphi = B_\theta = 0, \Psi = 0 \text{ under } \theta = 0.$$

3 Numerical method

For the numerical integration of the ideal MHD equations (2.1), we use Godunov-type conservative quasi-monotonic high resolution scheme [7], [8]. To guarantee divergence-free magnetic field it is applied the same procedure like in [9].

The equations system (2.1) integrated numerically in the region $R_{in} < R < R_{out}$, $0 < \theta < \pi/2$. It is taken non-uniform in the radial direction, being uniform in the polar angle

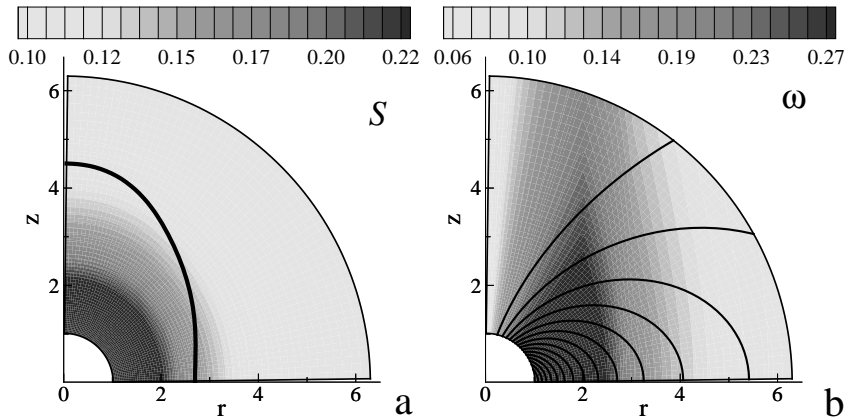


Figure 3: Distributions of $S(r, z)$, $\omega(r, z)$, $\Psi(r, z)$, $\beta = 1$, $t = 0$.

grid: $\omega_{R\theta} = \omega_R \times \omega_\theta$: $\omega_R = \{R_i = q^i R_{in}, i = -2, \dots, N_R + 2\}$, $q = 1 + \Delta\theta$, $\Delta\theta = \frac{\pi/2}{N_\theta}$, $\omega_\theta = \{\theta_j = j\Delta\theta, j = -2, \dots, N_\theta + 2\}$, $N_\theta = 60$, $N_R = 60$. The time step of the integration τ is restricted by Courant condition, $\tau = 0.25\tau_c$.

4 Results

For mathematical simulation of the interaction between a magnetic star and its accretion disk it has been performed several runs for different values of the magnetic diffusivity ζ . In figures 3 – 15 it is presented the results for the following values of parameter ζ : 0, 0.001, 0.002, 0.005.

Figure 3 shows the initial system configuration at time moment, $t = 0$. The background color in figure 3a shows the plasma specific entropy distribution $S(r, z)$, thick line – for the plasma parameter $\beta = \frac{p}{B^2/8\pi} = 1$. The background color on figure 3b shows the plasma angular velocity distribution $\omega(r, z)$, streamlines show magnetic field lines – magnetic flux function $\Psi(r, z)$.

The evolution of the coronal magnetic field loops in the star – disk system depends on the surface magnetic diffusivity ζ . One can pick out the characteristic features which are essential for this process. For all the cases, poloidal field lines are pulled out and reconnected periodically (each ten rotation period of the disk inner bound). Then, a magnetic field toroidal component is generated. After reconnection, a plasmoid is formed. It is surrounded by closed poloidal magnetic field lines along which the poloidal electric current is running. Plasmoid is determined by a strong toroidal magnetic field and a low gas pressure. The angular velocity inside the plasmoid is different from the corona one. $t = 50$ is chosen for presenting the simulation results (the time is measured in disk inner bound rotation period). Up to that moment, several reconnections of magnetic field lines took place, and next ejected plasmoid moves outwards to the outer bound. Previous series of reconnections already led to the opening of the field lines close to the rotation axis.

Figures 4a–f show the distributions of some variables for a magnetic diffusivity $\zeta = 0$.

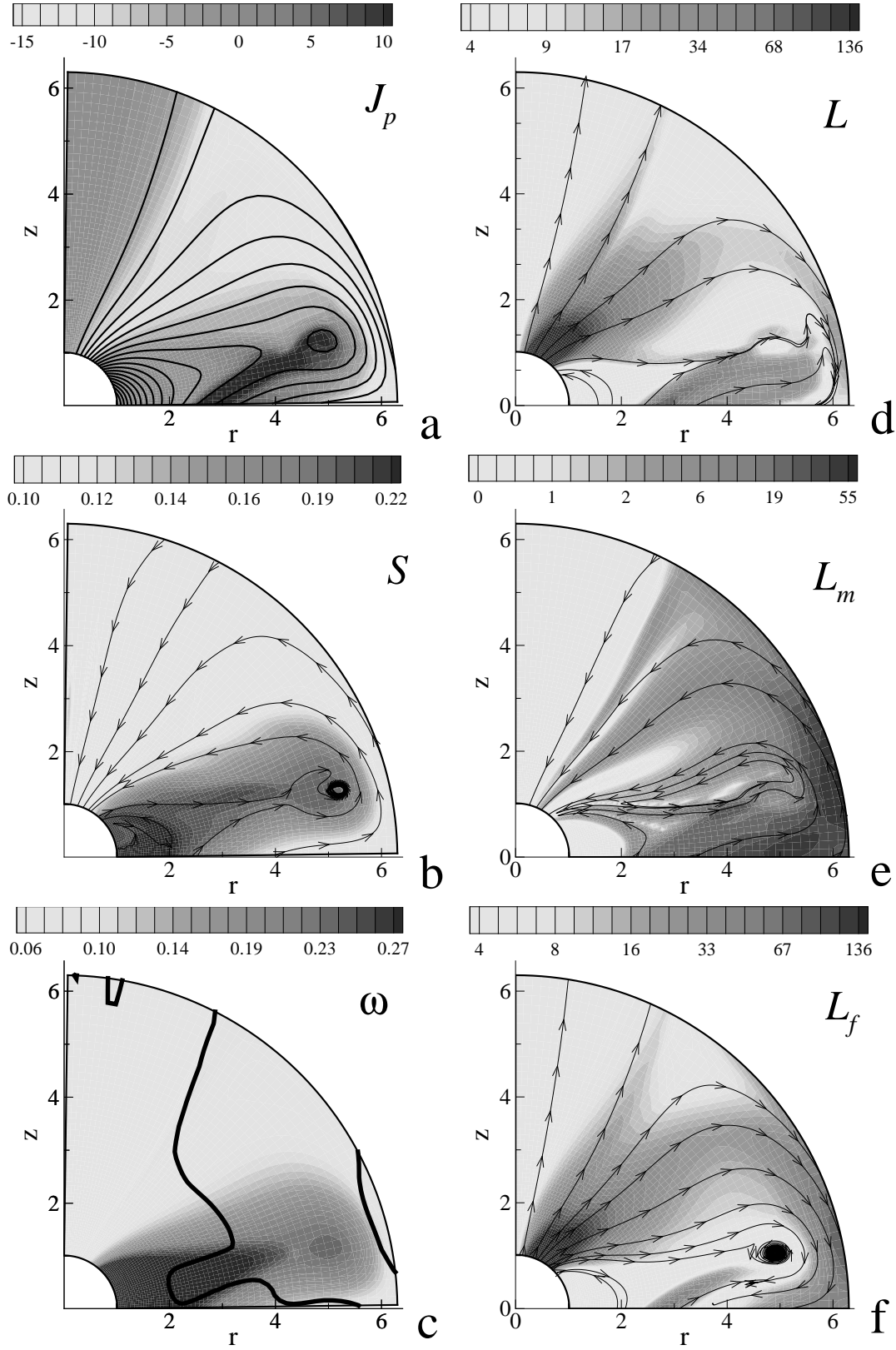


Figure 4: Distributions $S(r, z)$, $\omega(r, z)$, $\Psi(r, z)$, $\beta = 1$, $t = 50$.

The background colour on figure 4a shows the distribution of the poloidal current $J_p = rB_\varphi = R \sin \theta B_\varphi$. The magnetic field lines are shown also in this plot by firm lines. It is clear from these pictures that the initial configuration has essentially changed and now it is not dipole-like. In the disk differential rotation region ($r > 2$), field lines come out of its surface with large slope angle (more than 30°), fulfilling the conditions for matter outflow from the disk. A toroidal magnetic field is generated as a result of the differential rotation, implying that there is a poloidal current in the corona, forming a double current sheet (background dark colour area on figure 4a). In the neighborhood of the star poloidal current level, lines approximately coincide with the poloidal field ones, implying that the magnetic field is almost force-free.

The background colour on figure 4b shows the distribution of the specific entropy S . Streamlines present the matter current lines. It is clear that the matter flows into the plasmoid area from the disk and disk inner part. Plasmoid has hot matter surrounding it from the corona up to the outer boundary.

The background colour on figure 4c shows the plasma angular velocity distribution, firm line – plasma parameter level $\beta = 1$. It is evident from comparing figures 4a and 4c that the angular velocity is practically constant along the field lines, especially nearby the star. It means that in this area the generation of the toroidal magnetic field does not take place, i.e. there are not poloidal electric currents. The magnetosphere, rotating with constant angular velocity, gives angular momentum to the plasmoid, twisting the matter inside it.

Figures 4d – 4f show the distributions of several quantities that describe the angular moment transport in the system. The angular momentum conservation equation can be found from the continuity equation and is

$$\frac{\partial \rho l}{\partial t} + \text{div} \mathbf{L} = 0,$$

here $\rho l = \rho v r$ – angular momentum density. The poloidal components of the angular momentum flux density are

$$\mathbf{L} = R \sin \theta \left(\rho v_\varphi \mathbf{u}_p - \frac{B_\varphi \mathbf{B}_p}{4\pi} \right),$$

where \mathbf{u}_p , \mathbf{B}_p – plasma poloidal velocity and magnetic field. The first term in the right part describes angular momentum transported by matter, the second one – by magnetic field.

The background colour on figure 4d shows the magnitude of the angular momentum flux, and streamlines show the direction of the system angular momentum transport. There are two areas of intense momentum transport. One of them is nearby the star pole where transport takes place due to magnetic stresses (see figure 4f). The second one is above the disk, in its differential rotation area where the transport is caused by matter flow. These processes are presented on figures 4e,f in more detail. In figure 4e, streamlines show the angular momentum flux direction carried by matter. The background colour shows the magnitude of this vector. On figure 4f streamlines – angular momentum flux direction, carried by the magnetic field, by colour – its magnitude. It is clear from the figure 4f that angular momentum from the star is transported by magnetic field mainly. Also there is intense momentum transport inside the plasmoid.

The distributions for the same variables at $t = 50$ are shown on figures 5 – 7 for a finite surface magnetic diffusivity. Figures 5a – 5f correspond to $\zeta = 0.001$, figures 6a – 6f – $\zeta = 0.002$, figures 7a – 7f – $\zeta = 0.005$.

The figures 8 – 11 show the influence of the magnetic diffusivity on the magnetic field topology. Level lines of the magnetic flux function $\Psi(r, z)$ for all cases ($\zeta = 0$, $\zeta = 0.001$, $\zeta = 0.002$, $\zeta = 0.005$) are chosen at $t = 11$. At this time, the first reconnection took place for the case $\zeta = 0$. It is clear (see figures 8 – 11) that the less disk conductivity (i.e. more magnetic diffusivity), the more distance from axis and disk where the plasmoid ejection takes place. In case of finite disk conductivity, field lines are no longer frozen into the disk and, twisted by the star, they are shifted outwards. One can say that the more surface magnetic viscosity ζ , the slower the evolution takes place and plasmoids are formed more seldom in corona.

The matter flowing out from the disk and the magnetic field both take away the angular momentum from it. The whole angular momentum flux taken away from the disk per unit time is

$$L = L_m + L_f = - \int \rho[\mathbf{r}, \mathbf{u}]\mathbf{u}d\mathbf{S} + \frac{1}{4\pi} \int [\mathbf{r}, \mathbf{B}]\mathbf{B}d\mathbf{S}.$$

Here, integration is over the disk surface, $d\mathbf{S}$ – element of disk surface outwards directed (from the simulation region). The first term L_m is the angular momentum flux carried by matter, the second one L_f – angular momentum flux carried by magnetic field.

The time dependence of the angular momentum fluxes carried by matter L_m , by magnetic field L_f and their sum $L = L_m + L_f$ are shown on figures 12 – 15 for different values of ζ .

For $\zeta = 0$ (see figure 12), the process of angular momentum transport from the disk to the corona is quasi-periodic with period equal approximately to ten rotation period of the disk inner part. After $t_* = 45$ there is relaxation of the system accompanied by small oscillations of the angular momentum fluxes. During this time there is no new plasmoid generation. After $t = 65$, the reconnection process of the magnetic field lines are resumed. It can be seen from the angular momentum fluxes oscillations (see figure 12).

The finite disk conductivity changes the course of events (interaction between magnetic star and accretion disk). As it is seen from figures 12 – 15, the magnetic lines reconnection lasts until some time t_* (different for different ζ). The more magnetic diffusivity ζ , the plasmoids ejection later begins and earlier ends. Let us note that in case of a finite disk conductivity the coronal magnetic field evolution is qualitative similar to the perfect one. The reconnection of magnetic field lines takes place at the time corresponding to the maximum angular momentum outflow carried by magnetic field from the disk. In contrast to a perfect disk conductivity ($\zeta = 0$), the activity of the reconnection slows down and the system relaxes to a state such that there is no new plasmoid generation. The disk angular momentum carried by magnetic field gets balanced by angular momentum carried by matter. No disk–frozen magnetic field lines move along the disk and it lead to the increasing of the magnetic flux in the disk. In particular, that angular momentum flux carried by the magnetic field from the disk increases. The whole angular momentum flux becomes zero, i.e. $|L| \ll |L_f|$.

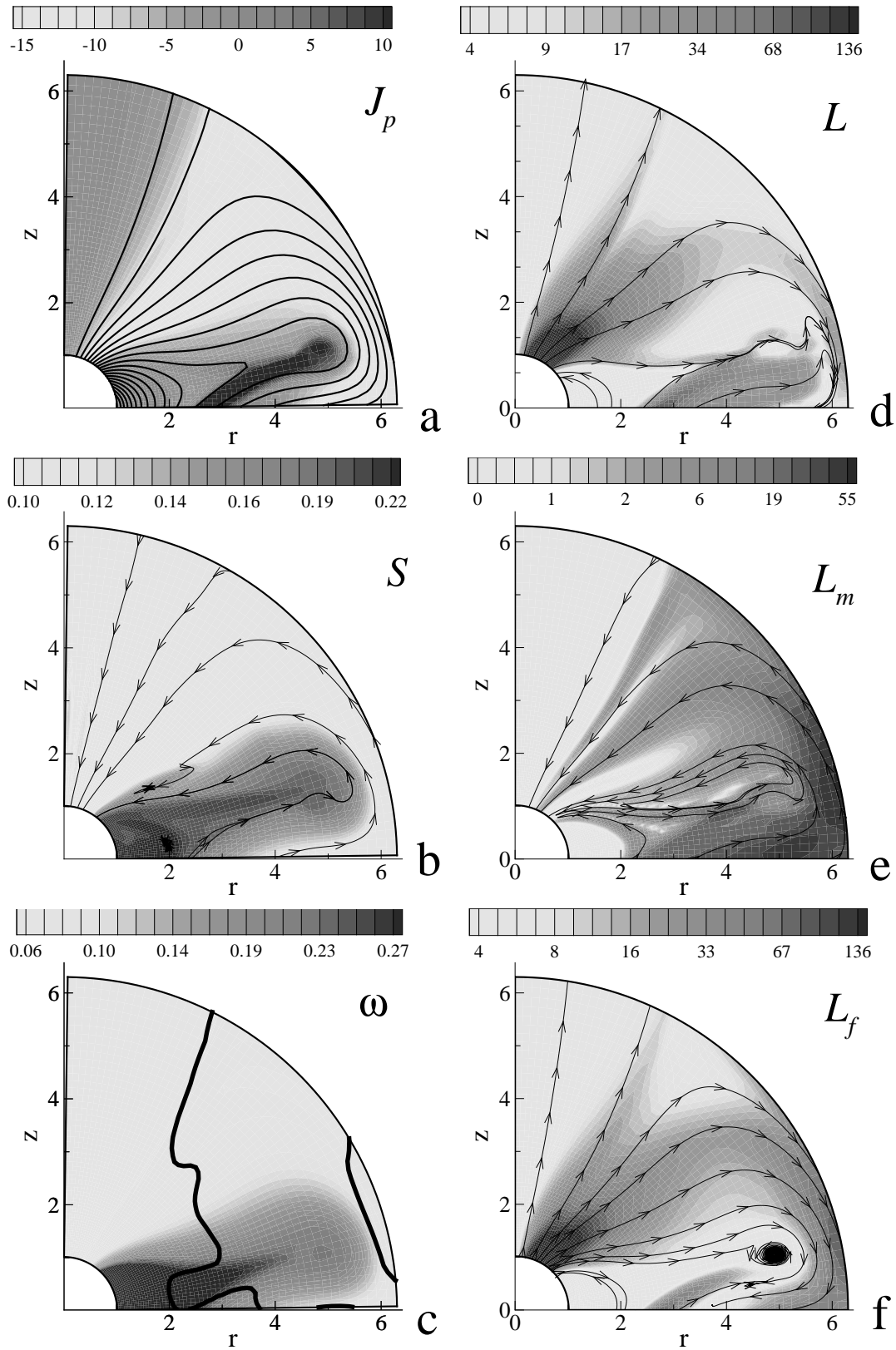


Figure 5: $\zeta = 0.001$, $t = 50$.

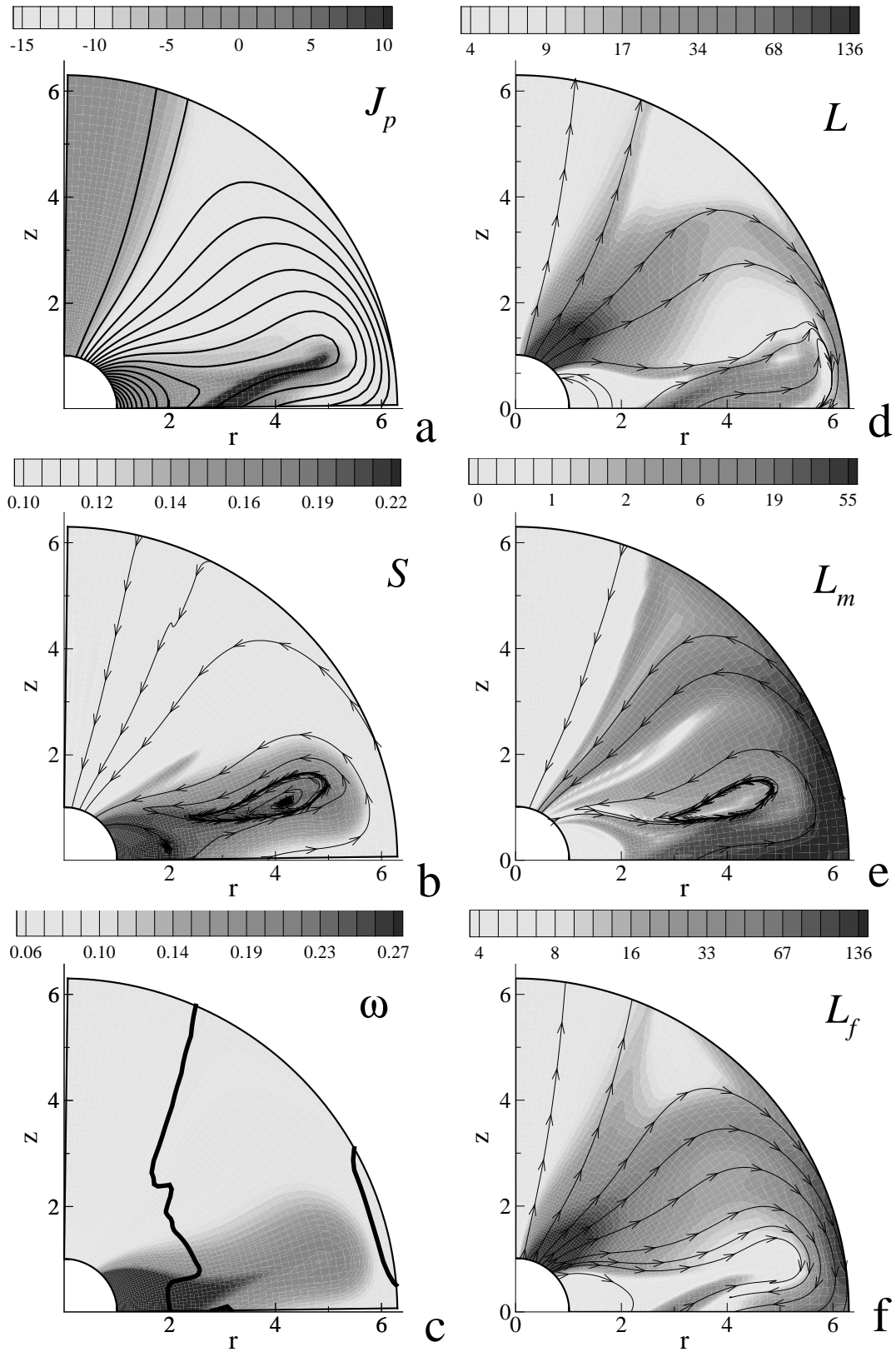


Figure 6: $\zeta = 0.002$, $t = 50$.

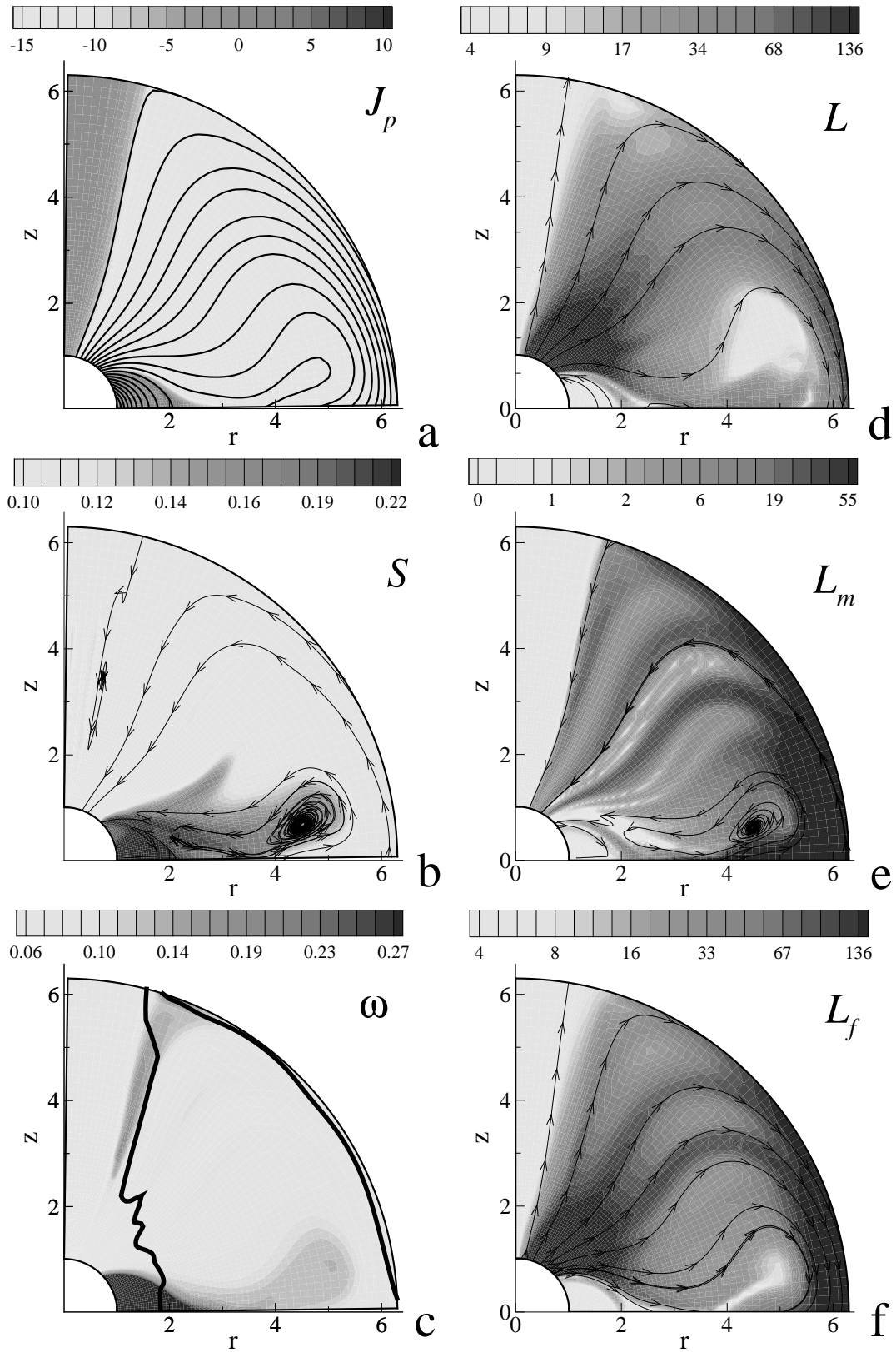


Figure 7: $\zeta = 0.005$, $t = 50$.

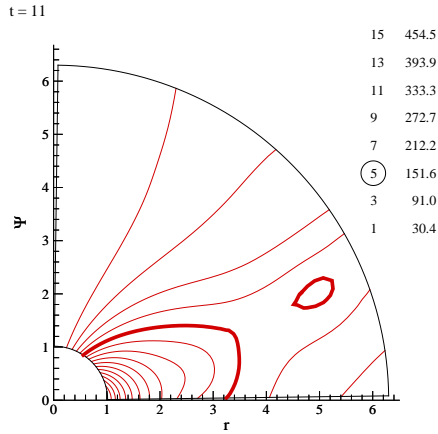


Figure 8: Magnetic field lines, $t = 11$, $\zeta = 0.0$.

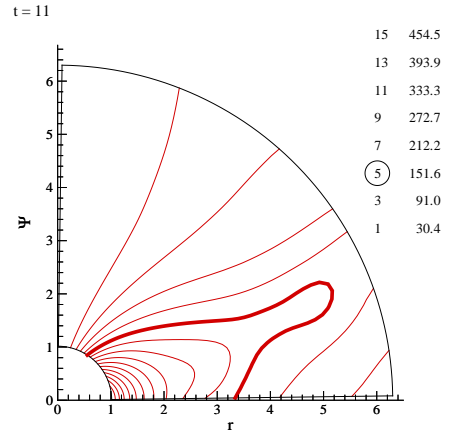


Figure 9: Magnetic field lines, $t = 11$, $\zeta = 0.001$.

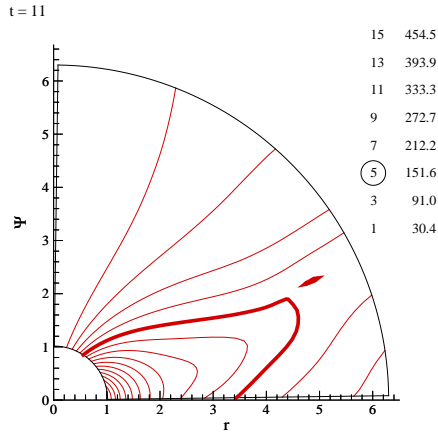


Figure 10: Magnetic field lines, $t = 11$, $\zeta = 0.002$.

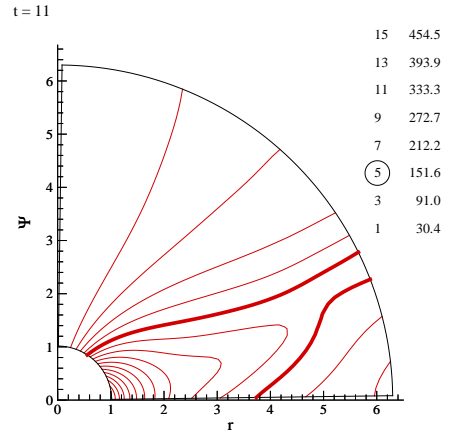


Figure 11: Magnetic field lines, $t = 11$, $\zeta = 0.005$.

5 Conclusions

The results of a simulation of the interaction between magnetic star and accretion disk for different disk surface magnetic diffusivity are presented. It has been determined that this process occurs with quasi-periodic reconnection of the magnetic field lines and plasmoid ejections. It has been studied the disk magnetic diffusivity influence on the star – corona – disk system evolution. In case of perfect disk conductivity the evolution of the coronal magnetic field leads to a periodic outflow of the angular momentum from the disk. Under finite disk conductivity, the configuration of the magnetic field lines is formed such that the angular momentum flux carried by the magnetic field from the disk becomes balanced by the flux transported by matter.

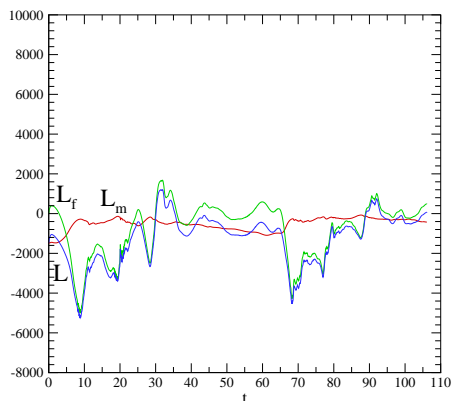


Figure 12: Angular momentum flux, $\zeta = 0.0$.

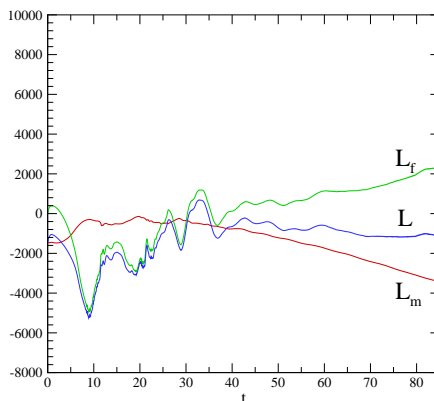


Figure 13: Angular momentum flux, $\zeta = 0.001$.

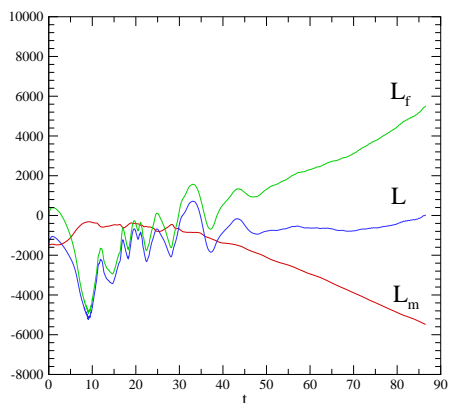


Figure 14: Angular momentum flux, $\zeta = 0.002$.

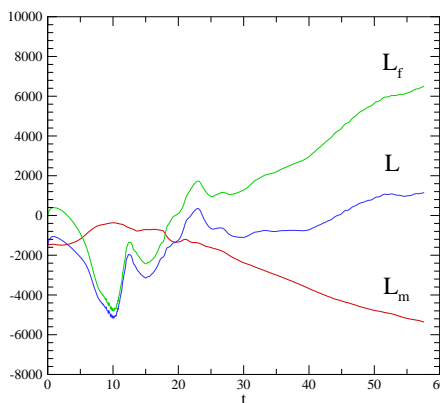


Figure 15: Angular momentum flux, $\zeta = 0.005$.

References

- [1] *Shakura N.I., Sunyaev R.A.* Black holes in binary systems. Observational appearance. *Astronomy and Astrophysics*, 1973, V.24, p. 337-355.
- [2] *Balbus S.A.* Enhanced angular momentum transport in accretion disks. *Annual Review of Astronomy and Astrophysics*, 2003, V. 41, p. 555-597.
- [3] *Bisnovatyi-Kogan G.S., Lovelace R.V.E.* Advective accretion disks and related problems including magnetic fields. *New Astronomy Reviews*, 2001, V.45, p. 663-742.
- [4] *Hawley J.F., Gammie C.F., Balbus S.A.* Local three-dimensional magnetohydrodynamic simulations of accretion disks. *Astrophysical Journal*, 1995, V. 440, N 2, p. 742-763.

- [5] *Blandford R.D., Payne D.G.* Hydromagnetic flows from accretion discs and the production of radio jets. MNRAS, 1982, V. 199, p. 883-903.
- [6] *Landau L.D., Lifshitz E.M.* Electrodynamics of continuum medium. Volume VIII, M, Nauka, 1982, 620 p.
- [7] *T.G. Yelenina, G.V. Ustyugova.* Simulation of the MHD-flows generated by moving of the conducting plane in the perfect conducting plasma. Preprint Keldysh Inst. Appl. Math. RAS, 2004, N 73, 25 p.
- [8] *Galanin M.P., Yelenina T.G.* Nonlinear monotization of difference schemes for linear advection equation. Preprint Keldysh Inst. Appl. Math. RAS, 1999, N 44, 30 p.
- [9] *Tóth G.* The $\nabla \cdot \mathbf{B}$ constraint of some flux corrected transport and total variation diminishing numerical schemes for hydrodynamic and magnetohydrodynamic problems. J. Comput. Phys., 2000, V.161, N 2, p. 605-652.